ChemPubSoc Europe

DOI: 10.1002/cphc.201800937

CHEMPHYSCHEM Articles

Matrix-induced Linear Stark Effect of Single Dibenzoterrylene Molecules in 2,3-Dibromonaphthalene Crystal

Amin Moradi[+],[a] Zoran Ristanović[+],[a] Michel Orrit,*[a] Irena Deperasińska,[b] and Bolesław Kozankiewicz*[b]

Absorption and fluorescence from single molecules can be tuned by applying an external electric field – a phenomenon known as the Stark effect. A linear Stark effect is associated to a lack of centrosymmetry of the guest in the host matrix. Centrosymmetric guests can display a linear Stark effect in disordered matrices, but the response of individual guest molecules is often relatively weak and non-uniform, with a broad distribution of the Stark coefficients. Here we introduce a novel single-molecule host-guest system, dibenzoterrylene (DBT) in 2,3-dibromonaphthalene (DBN) crystal. Fluorescent DBT molecules show excellent spectral stability with a large linear Stark effect, of the order of 1.5 GHz/kVcm^{-1}, corresponding to an electric dipole moment change of around 2 D. Remarkably, when the electric field is aligned with the *a* crystal axis, nearly all DBT molecules show either positive or negative Stark shifts with similar absolute values. These results are consistent with quantum chemistry calculations. Those indicate that DBT substitutes three DBN molecules along the *a*-axis, giving rise to eight equivalent embedding sites, related by the three glide planes of the orthorhombic crystal. The static dipole moment of DBT molecules is created by host-induced breaking of the inversion symmetry. This new host–guest system is promising for applications that require a high sensitivity of fluorescent emitters to electric fields, for example to probe weak electric fields.

1. Introduction

Fluorescent polycyclic aromatic hydrocarbons (PAHs) are recently receiving increasing attention as bright and photostable single-photon emitters that can be integrated into on-chip quantum electronic devices.[1–4] Single-molecule fluorescence spectroscopy of PAHs at cryogenic temperatures has been used as a highly sensitive technique to optically probe the interactions of individual emitters with their local environments.[5–7] The spectral position of the narrow optical transitions (typical linewidth 30–50 MHz) is very sensitive to external perturbations, for example from electric fields. The shift in the spectral transition frequency between the ground and the excited state of a molecule in an electric field is commonly known as the Stark effect. Typically, the frequency shift has both linear and quadratic Stark contributions which depend on the change in electric dipole moment and in polarizability tensor, respectively, between the excited and ground states.[8,9] Several host-guest systems with different contributions of the linear and quadratic Stark effects have been reported in the literature.[10–15] These studies mostly concentrated on centrosymmetric fluorescent emitters that should exhibit a quadratic Stark effect only. However, the central symmetry of the guest molecules is often broken in disordered host matrices, such as polymers, making it possible to observe the linear Stark effect.[9] For terrylene in *p*-terphenyl, flipping of a host phenyl ring close to the guest leads to switching from a centrosymmetric to a non-centrosymmetric insertion, with distinct quadratic and linear dependences.[11,16] Nevertheless, a broad distribution of the linear Stark coefficients (often centered around zero) and low linear Stark coefficients for the majority of emitters still remain serious experimental limitations. For applications where the transition frequency should be tuned by an applied electric field, it is highly desirable to have a large fraction of single emitters responding uniformly (i.e. with similar Stark shifts) to the applied electric field. Furthermore, as the quadratic Stark effect is very weak in nature, the large linear Stark effect is advantageous. Such probes would enable faster and more reproducible tuning of single-photon emission, as well as a higher sensitivity of single molecules to small perturbations by local electric fields, including the optical detection of single electrons.[17–19]

Many of the probe molecules in single-molecule spectroscopy, such as dibenzoterrylene (DBT),[20] are centrosymmetric, which means that they do not intrinsically possess a permanent electric dipole moment. DBT has been recently a popular choice

[a] *A. Moradi,[+] Dr. Z. Ristanović,[+] Prof. Dr. M. Orrit*
Huygens-Kamerlingh Onnes Laboratory, LION, Postbus 9504, 2300 RA Leiden, The Netherlands
E-mail: Orrit@Physics.LeidenUniv.nl
[b] *Dr. I. Deperasińska, Prof. Dr. B. Kozankiewicz*
Institute of Physics, Polish Academy of Sciences Al. Lotnikow 32/46, 02-668 Warsaw, Poland
E-mail: kozank@ifpan.edu.pl
[+] *These authors contributed equally to the work.*

Supporting information for this article is available on the WWW under https://doi.org/10.1002/cphc.201800937

for fluorescent studies due to its excellent photophysical properties, including high brightness, photostability, single-emitter coupling to waveguides and to on-chip cavities,[21–23] and single-photon emission.[24]

A tunable single-molecule emission of DBT in the electric field can further facilitate quantum manipulation and integration of this molecule into molecular electronic quantum devices. Because they are easily synthesized, chemically identical and reproducible, single-molecule-based quantum emitters offer an appealing alternative to more frequently used single-photon sources, such as color centers in diamond, quantum dots, and other solid-state systems.[25–27] However, the well-studied and the most used molecular-based system, DBT in anthracene, mainly exhibits quadratic Stark effect with very small linear coefficients (due to crystal defects) that are distributed around zero.[28] One strategy to induce a permanent electric dipole of the guest molecule is by the chemical synthesis of an asymmetric dye molecule.[29] Another strategy is to insert the symmetric guest molecule into a crystal built from asymmetric host molecules. This latter strategy is not risk-free, as the insertion of the guest into the host molecular crystal should not induce further defects nor any significant spectral diffusion.[30] The resulting doped crystals ideally should preserve the desirable spectral properties of the low-temperature fluorescent probe, such as narrow optical transitions, high spectral stability and low spectral diffusion. Recent experimental and quantum chemistry studies on terrylene in di-substituted naphthalenes, such as 2,3-dichloronaphthalene and 2,3-dibromonaphthalene (DBN for short), have shown that these dihalogenated compounds can be suitable hosts for fluorescent PAH molecules.[31,32] Here we show that the electronegativity of halogen atoms, combined with the herring-bone crystalline structure of the host, is able to induce large electric dipoles on a centrosymmetric molecule such as dibenzoterrylene. We introduce a novel host-guest system based on DBT in DBN and report for the first time on a large linear Stark shift homogeneously affecting all fluorescent molecules by matrix-induced symmetry breaking.

Experimental Section

Crystal Growth

DBN used in this work was purchased from Ark Pharm Inc. High-quality single crystals of zone-refined DBN doped with DBT molecules were obtained by co-sublimation at ~0.2 bar of argon gas. To prevent perturbations from the convection flow in the sublimation chamber, the sublimator was kept horizontal during growth. The sublimation-grown crystals develop along the (*a*,*b*) plane as thin mm-sized plates or flakes, with a typical thickness of few microns along the *c*-axis.

Optical Microscopy

A well-defined single crystal free of visible defects was carefully transferred to a silica substrate on which interdigitated gold electrodes had been deposited by lithography (see Figure 1b). The electrodes were 200 nm thick and were separated by a distance of

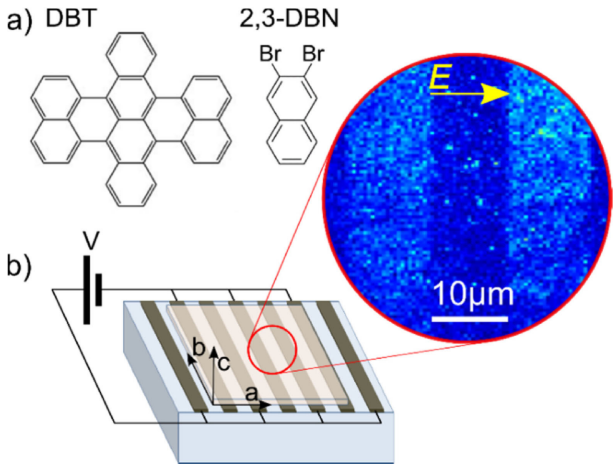

Figure 1. a) Molecular structures of DBT and 2,3-DBrN. b) Schematic of the chip for Stark effect measurements with a crystal placed on the top of electrodes. The axes designate the crystallographic orientation of the crystal in the plane of electrodes. Zoom-in shows a confocal fluorescence microscopy image of the crystal containing fluorescent DBT molecules. The electrodes are visible through stronger light scattering.

10 µm. The external electric field was varied through the voltage applied to the electrodes. The crystals were placed on the chip at the desired angle between the electric field and the crystallographic *a*-axis, determined by separately measuring the orientation of the transition dipole moment of DBT impurities. To this aim, the crystal was placed on a rotating stage and excited at normal incidence by a 756 nm laser beam with linear polarization in the (*a*,*b*)-plane of the crystal. Fluorescence images were recorded with a sensitive CMOS camera (Hamamatsu, Orca Flash 4.0) while rotating the stage.

All single-molecule measurements were done at 1.2 K in a home-built liquid-helium bath cryostat. Single DBT molecules were excited by a tunable continuous wave Ti:Sapphire laser (Coherent, 899–21) with a 2 MHz bandwidth. The sample was scanned in a confocal arrangement using a scanning mirror (Newport, FSM-300-01). The fluorescence light was collected by a cryogenic objective (Microthek, NA = 0.8) and detected by a single-photon counting module (Excelitas Single Photon Counting Module, SPCM-AQRH-16) with a set of filters (Chroma HQ760LP and Semrock FF02-809/81) in the detection path.

Bulk fluorescence excitation and emission spectra were obtained at 5 K using a Ti:Sapphire laser (Coherent, Mira-HP). For the detection path, a scanning monochromator (McPherson, 207) and a photomultiplier (EMI, 9659) operating in photon-counting mode were used. The fluorescence excitation spectrum was obtained by scanning the laser while the monochromator was set to 773.6 nm (a band pass filter Chroma D780/20 was used in the detection path). For the fluorescence emission spectrum the laser was in resonance with the vibronic component located at 740.3 nm (with Semrock FF01-785/62 filter in the detection path).

Quantum Chemistry Calculations

All calculations in this work were done with the Gaussian 09 package.[33] Like in our previous works[32,34] optimization of the geometry of DBT placed inside the rigid crystalline lattice was done with the aid of the ONIOM(B3LYP/6-31G(d,p):UFF) procedure, where B3LYP/6-31G(d,p) is used for the DBT molecule (as so-called high layer in the division of the calculated system) and UFF method for

the DBN lattice (low layer). In our calculations we consider a crystal composed by 3×2×2 unit cells (i.e. 96 molecules of DBN) with geometry based on the orthorhombic P_{bca} unit cell of DBN crystal, as described in previously published crystallographic data.[32,35] A DBT molecule replaces three molecules of DBN aligned along the crystal *a*-axis. Calculations were strongly limited by the requirements of the computational memory and time, especially for the electronically excited states. Therefore, the simplest TD B3LYP/STO-3G method was used for calculations of the dipole moments of both, the whole system and the individual components.

2. Results

2.1. Photophysical Properties of the System

The molecular structures of DBT and DBN are shown in Figure 1a. A platelet-like crystal of DBT/DBN was optically contacted to a custom-made glass chip with electrodes (Figure 1b). First we studied the bulk photophysical properties of the DBT/DBN system. Figure 2a displays the bulk fluorescence excitation (blue curve) and

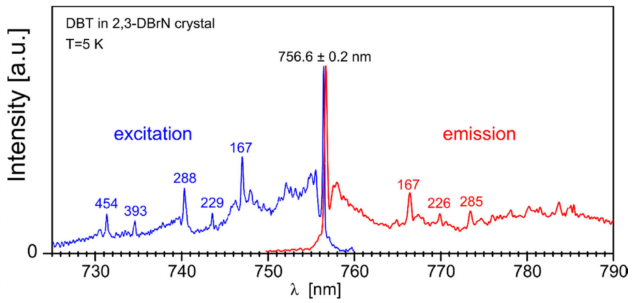

Figure 2. Fluorescence excitation spectrum (blue) with fluorescence detection at wavelengths longer than 773.6 nm, and fluorescence spectrum (red) excited at 740.3 nm. The number above each vibronic line indicates the vibration frequency (shift from the ZPL) in reciprocal centimeters (cm^{-1}).

emission (red curve) spectra of DBT/DBN. A single, inhomogeneously broadened line at about 756.6 nm is found at the same wavelength in the excitation and fluorescence spectra. Thus, it indicates a purely electronic zero-phonon line (ZPL) of this system, and it was the only one we could find. The inhomogeneous linewidth of the ZPL is ~5 cm^{-1}. The absence of other resonant absorption and fluorescence peaks points towards a *single spectroscopic site* in this host-guest system.

For the cryogenic single-molecule experiments, the laser was tuned at 756.4 nm to excite individual DBT molecules from the ground vibronic level of the ground state ($|g,\nu=0\rangle$) to the ground vibronic level of the excited electronic state ($|e,\nu=0\rangle$). In the following, we will use the static dipole moment vectors $\boldsymbol{\mu}_g$ and $\boldsymbol{\mu}_e$ in the ground and excited state, respectively, as well as their difference $\Delta\boldsymbol{\mu}=\boldsymbol{\mu}_e-\boldsymbol{\mu}_g$. The transition matrix element between these two states is another vector, noted $\boldsymbol{\mu}_{eg}$. The studied system also provided a conveniently large number of single emitters within a 3 GHz single frequency scan. Figure 3a shows the excitation spectra of more than 20 DBT molecules recorded over 250 s of repetitive frequency scans. Each horizontal line indicates an individual DBT molecule within the focal spot of the laser beam, showing excellent spectral stability in time. No significant frequency jumps or spectral diffusion have been observed, even during longer measurements. Similarly, we did not observe significant broadening of the homogeneous linewidth, as shown

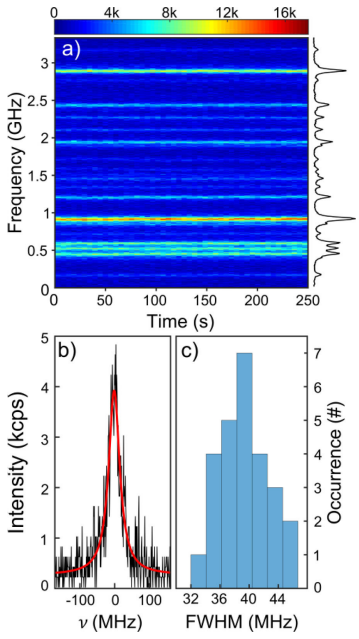

Figure 3. a) Time traces of more than 20 single molecules measured at 756.4 nm. The color scale units are counts per second. b) Single DBT molecule ZPL spectrum fitted with the Lorentzian profile. c) Histogram of the single-molecule homogeneous linewidth.

for a single molecule in Figure 3b. The full width at half-maximum (FWHM) was extrapolated from the measured saturation curves of 30 molecules (Figure 3c). The average FWHM of 37±4 MHz agrees well with the observed fluorescence lifetime of DBT in DBN, 4.84 ns (see Figure S1 in the Supporting Information). The number of detected counts at saturation was around 80,000 cps for most molecules, a typical detection rate for well-oriented DBT molecules.[20] These measurements already indicate very favorable photophysical properties of the DBT/DBN system for single-molecule spectroscopy. We point out here that the size of the host halogen atoms most likely also plays a role in stabilizing the system. We performed similar experiments with 2,3-dichloronaphthalene as host, but DBT molecules in this system turned out to be significantly less photostable. The introduction of halogen atoms to the aromatic host could be a common strategy to induce a linear Stark shift. Türschmann et al. have reported linear Stark effect on DBT in *para*-dichlorobenzene, although the authors noted that different individual DBT molecules in this system respond differently to the electric field.[36]

2.2. Stark Effect Experiments

The Stark shift of single-molecule ZPLs was measured by applying a variable voltage on the electrodes. In all Stark measurements the applied electric field varied from −1 kV/cm to 1 kV/cm while the laser was scanned for each voltage applied. The uniformity of the electric field was ensured by measuring molecules at the distance of 5±1 μm from the edges of the electrodes and within the same focal plane as the electrodes (Figure 1b). Figure 4a presents the Stark shift of more than 20 DBT molecules when the *a*-axis of the crystal was aligned along the applied electric field. The large linear Stark shifts in the order of 1.5 GHz/kVcm^{-1} proved that the strategy of inducing static dipole moments in the guest molecules by the use of asymmetric host molecules is effective. Remarkably, all molecules within the scanned confocal volume exhibited similar absolute values of the Stark coefficients, as shown in Figure 4b. We

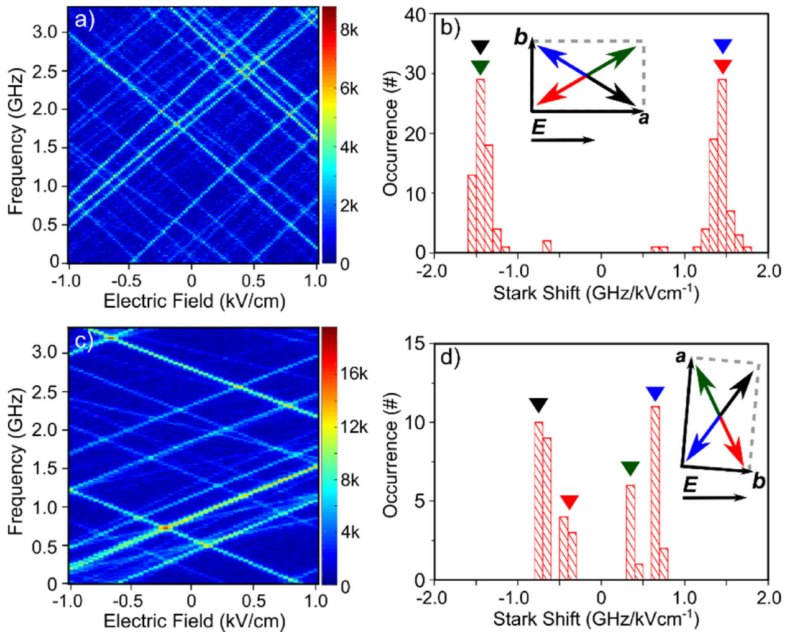

Figure 4. Stark shifts of DBT single molecules in an electric field nearly parallel or perpendicular to the *a*-axis. a) Electric field nearly parallel ($2\pm5^\circ$) to the *a*-axis, and b) corresponding histogram of the Stark shift. c) Electric field nearly perpendicular ($85\pm5^\circ$) to the *a*-axis, and d) corresponding histogram of the Stark shift. The color scales in (a) and (c) are in counts per second. Insets in (b) and (d) indicate the orientation of the crystal (and 4 molecular dipoles) in the (a,b) plane with respect to the electric field, ***E***. The color-coded triangles indicate the values of the Stark shifts for the corresponding four dipoles.

find two distinct sub-populations of molecules, but with identical absolute values of their Stark shift (±1.4 GHz/kVcm^{-1}). The opposite slopes of the two sub-populations indicate that the electric dipole difference vector, $\Delta\boldsymbol{\mu}$, can have either a positive or a negative projection onto the applied electric field, directed along the *a*-axis. Previously, large linear Stark shifts of similar magnitudes were observed on single molecules of terrylene in amorphous polyethylene (up to 2 GHz/kVcm^{-1}).[9] In crystalline hydrocarbon matrices, such as naphthalene, *p*-terphenyl and *n*-hexadecane, the Stark shifts of terrylene and dibenzathranthrene are comparatively weak, with the highest recorded linear coefficients in the order of 200 MHz/kVcm^{-1}.[10,11,13] In stark contrast to these previous studies, almost all molecules in our system exhibit equally large linear Stark shifts, without any non-responsive molecules. Such a large and homogenous response of all emitters to an external electric field has never been reported previously.

Further inspection of the crystal orientation in the electric field shows that the magnitudes of the Stark shift depend on the exact alignment of the crystal in the electric field. As expected, the minimum in the Stark response is reached when the crystallographic *a*-axis is nearly perpendicular to the electric field (Figure 4c). For an arbitrary orientation of the crystal with respect to the electrodes, we found four distinct sub-populations of molecules with different Stark shifts, and two-by-two opposite values. For example, for an angle $\varphi\sim85^\circ$ between the electric field and the *a*-axis, we find Stark shifts centered around ±0.4 and ±0.7 GHz/kVcm^{-1}, as shown in Figure 4d. This result suggests at least 4 distinct dipole orientations in the electric field, related to each other by the symmetry on the crystal. Interestingly, the maximum value of the Stark coefficient (1.56 GHz/kVcm^{-1}) is reached for a crystal with an angle φ of 20° between the *a*-axis and the electric field (Figure S3). The measured Stark coefficient maximum translates into the electric dipole moment change of 2.1 D, if a local-field correction factor of 1.5 is applied.

We can now consider our results as a special case of four dipoles in an electric field ***E*** situated in the (*a,b*) plane, which is our experimental arrangement. The linear Stark shift is proportional to a scalar product of $\Delta\boldsymbol{\mu}$ and ***E***, i.e., $h\Delta\nu=-\Delta\boldsymbol{\mu}\cdot\boldsymbol{E}$. Here we consider the effective electric field which includes the local-field correction. As discussed later, the symmetries of the host crystal give rise to four possible projections of the dipole moment onto the field, which can be expressed using the angle φ between the electric field and the crystal's *a*-axis, as well as the angle θ between the *a*-axis and the $\Delta\boldsymbol{\mu}$ a particular molecule taken as a reference (see Figure 5). Note that θ is an intrinsic property of the crystal, whereas we can give φ arbitrary values by orienting the crystal with respect to the electrodes. By using the two angles θ and φ, the Stark shift will be different for each of the four *differently oriented* guest dipoles. The Stark shift of the reference molecule will then be $h\nu=-\Delta\boldsymbol{\mu}_{\max}\cdot\boldsymbol{E}\cos(\varphi+\theta)$ or expressed as the frequency change, $\Delta\nu=\Delta\nu_{\max}\cos(\varphi+\theta)$. For the three other molecules deduced by mirror symmetries on glide planes *(a,c)* and *(b,c)*, the shifts are: $\Delta\nu=\Delta\nu_{max}cos(\varphi-\theta)$, $\Delta\nu=-\Delta\nu_{max}cos(\varphi+\theta)$, $\Delta\nu=-\Delta\nu_{max}cos(\varphi-\theta)$, corresponding to four possible orientations of the dipole moments in the *(a,b)* plane.

Figure 5 shows the dependence of the Stark shift on the tilt angle φ of the crystal's *a*-axis with respect to the electric field. The calculated Stark shift as a function of φ (solid lines) coincided with the experimental data (circles) for $\theta=20\pm5^\circ$. Other values of θ could not match our results, as shown in Figure S4. The results also show that the four values of the Stark shift should merge into two values when the crystal is perfectly aligned with the electric field ($\varphi=0^\circ$), which is the case for the measurement shown in Figure 4a. The maximum of the Stark shift will be, however, recorded for the alignment angle $\varphi=-\theta$, when ***E*** coincides with one of the four projections of $\Delta\boldsymbol{\mu}$ vectors. These experimental findings will be generalized for an arbitrary electric field in the Discussion section.

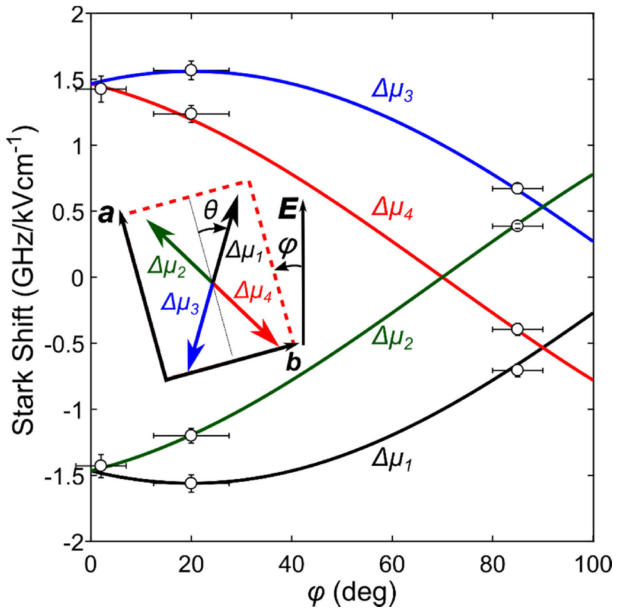

Figure 5. Angle-dependent Stark shift as a function of the angle, φ, between the a crystallographic axis and the electric field. The Stark shift is calculated for four electric dipoles (rotated by $-\theta+\varphi,\ \theta+\varphi, \pi-\theta+\varphi,\ \pi+\theta+\varphi$ and compared to the experimental data (hollow circles). The simulated values are determined for the maximum of the Stark shift 1.56 ± 0.06 GHz/kVcm^{-1} and $\theta=20^\circ$. The inset illustrates the orientation of the four dipoles used in calculation; *a* and *b* axes, electric field vector ***E***, as well as angles θ and φ are shown.

2.3. Quantum Chemistry Calculations

To understand the origin of the large Stark shift of DBT, we have performed quantum chemistry calculations looking for the structure of a DBT molecule and its dipole moments, which may be affected by interaction with the surrounding DBN host molecules. In the calculations, a guest DBT molecule was embedded in a P_{bca} orthorhombic unit cell of DBN (Figure S5) by replacing 3 host molecules along the crystal *a*-axis and was surrounded by 96 DBN molecules (12 elementary cells). The result of ONIOM(B3LYP/6-31G(d,p):UFF) optimization is shown in Figure 6a (for coordinates of the optimized DBT see Tab. S1). It is visible that the embedded DBT molecule loses the C_{2h} symmetry characterizing the isolated DBT.[37]

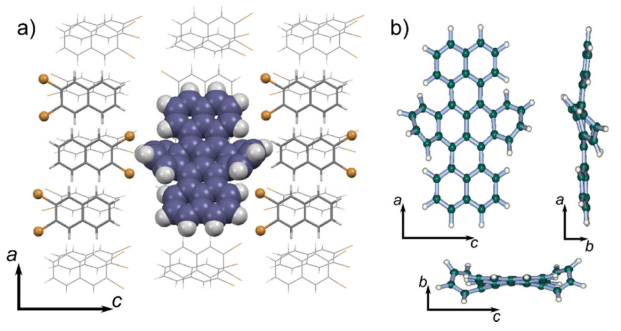

Figure 6. a) Insertion site, visualized in the (*a*,*c*) plane. The DBT molecule is represented in space-fill molecular model, replacing 3 host molecules; the adjacent DBN molecules (along *a*-axis) are highlighted as capped sticks. Bromine atoms (golden balls) are highlighted for convenience. b) Host-induced distortion and bending of the guest DBT molecule visualized in all three planes. For more detailed crystallographic information about the unit cell of the host matrix, see Figure S5.

Figure 6b illustrates the resulting large distortion of the terrylene core and the tetracene unit of DBT.

Structural changes of the DBT molecule are accompanied by changes of the static dipole moments in the ground and excited states. A free-space DBT molecule does not possess any permanent dipole moment. The total dipole moment of each unit cell of the DBN crystal (containing 8 DBN molecules) is also zero, although each of the DBN molecules has a non-zero dipole moment (1.48 D). Creating an empty cavity in the DBN crystal by removing three DBN molecules along the axis *a* results in the appearance of a dipole moment of 1.8 D, directed mainly along the *a* crystal axis (see Tab. S3). The asymmetric distribution of the electron density at the DBT molecule (with the DBN crystal optimized structure) has relatively large components of the electric dipole moment along the two crystal axes (*a* and *c*), as shown in Tab. S2. The total dipole moment of the whole system, i.e. DBT in DBN crystal, after optimization of DBT structure is 2.46 D (Tab. S3). The difference between dipole moment vectors of the crystal with the empty cavity and with the cavity filled with DBT is 1.53 D. This value is greater than the dipole moment calculated for the isolated DBT molecule in its crystal-deformed geometry, 0.69 D (Tab. S2). Thus, the interaction of DBT (in the electronic ground state) with the surrounding DBN molecules leads to a significant increase of the dipole moment of the whole system.

The isolated DBT molecule in the distorted geometry optimized in the DBN crystal also possesses a nonzero permanent dipole moment in the excited singlet S_1 state, equal 0.38 D according to our calculations (Tab. S2). The calculated difference between dipole moments in excited S_1 and ground S_0 electronic states is $|\Delta\boldsymbol{\mu}| =$ 0.47 D. The transition moment $\boldsymbol{\mu}_{eg}$ reaches 7.8 D and is oriented almost perfectly along the molecule's long axis (Tab. S2), as found experimentally. An interesting observation is that the vector difference $\Delta\boldsymbol{\mu}$ responsible for the large Stark effect, is directed mainly along the transition dipole moment $\boldsymbol{\mu}_{eg}$ (and thus along the *a*-axis of the host crystal).

Unfortunately, the size of the system required to calculate the dipole moment in the electronic excited S_1 state has to be much smaller than for the ground S_0 state. Therefore, the S_1 calculations were performed for a limited number of 28 surrounding host molecules, with the DBT geometry optimized in the ground state. Summarizing these results in Table 1 we may conclude that the dipole moment in the excited S_1 state increased by about 1 D, which is larger than the value calculated for the isolated DBT in the optimized geometry. Similar results were obtained with smaller simulation cells (Supporting Information Table S4). The projection of $\Delta\boldsymbol{\mu}$ onto the crystal *a*-axis is found to be 0.76 D, with an angle of 10° between the *a*-axis and $\Delta\boldsymbol{\mu}$ see Table 1). This value matches reasonably well with $\theta=20^\circ$ derived from the experiment.

Table 1. Components along the crystal axes of the transition dipole moment $\boldsymbol{\mu}_{eg}$ and dipole moments $\boldsymbol{\mu}_g$, $\boldsymbol{\mu}_e$, $\Delta\boldsymbol{\mu}=\boldsymbol{\mu}_e-\boldsymbol{\mu}_g$ of DBT obtained for the simulation cell with 28 host molecules (see Table S4 for details). All values are in D (where $1D=3.34\cdot10^{-30}$ Cm); *a-, b-, and c-*axis, represent the projections of the calculated vectors on the crystallographic axes of the crystal, whereas $|\boldsymbol{\mu}|$ represents the modulus of the corresponding vector.

	a-axis	*b-axis*	*c-axis*	$\lvert\mu\rvert$
$\boldsymbol{\mu}_{eg}$	8.0150	0.3820	0.4592	8.0372
$\boldsymbol{\mu}_g$	−0.6149	−0.6587	−7.7383	7.7906
$\boldsymbol{\mu}_e$	0.1438	−0.7913	−8.4195	8.4579
$\boldsymbol{\mu}_e-\boldsymbol{\mu}_g$	0.7587	−0.1326	−0.6812	1.0282

3. Discussion

Before discussing possible DBT insertions in the DBN crystal, let us briefly recall the structure of this crystal. DBN crystallizes in the orthorhombic P_{bca} system, which is characterized by three glide planes, with glide mirrors (*a,b*), (*b,c*), (*c,a*), and a center of symmetry at the center of the unit cell. The unit cell contains 8 molecules arranged in a herring-bone pattern. These molecules are all related by mirror symmetries in the glide planes, as illustrated in Figure S5. The 8 molecules in the unit cell thus cover all the 8 possible images of any particular molecule in the 3 glide planes (i.e., after suitable translations, see Figure S5), in the 3 screw axis rotations, which are products of two glide mirror symmetries, and in the inversion. Embedding a DBT molecule in this crystal requires removing 3 host molecules. Quantum chemistry calculations indicate that the most favorable way to do this is to replace 3 DBN molecules along the crystallographic *a*-axis (Figure 6a). Indeed, this is in accordance with the experimental finding that the DBT transition dipole moment, directed along the long DBT axis, is roughly aligned along the *a*-axis of the crystal. Taking the crystal structure into account, we find that the substitution can be realized in 8 different manners, taking each molecule in the DBN unit cell as the starting point for the substitution of 3 DBN molecules along the *a*-axis. Moreover, these 8 distinct insertion sites are all related by the same mirror symmetries in the glide planes as the original host molecules. Therefore, they are completely equivalent from a spectroscopic point of view, which nicely explains why only one single spectroscopic site is observed (Figure 2).

Let us now consider any vector $\boldsymbol{V}$ (components V_a, V_b, V_c in the crystal's orthonormalized reference frame) related to a molecule (1) in the DBN unit cell (see Figure S5). The associated vectors for each of the seven other molecules will be deduced from $\boldsymbol{V}$ through mirror symmetries and their products, leading to 8 vectors with components $\pm V_a$, $\pm V_b$, $\pm V_c$. In particular, the Stark effect is determined by the dipole moment change $\Delta\boldsymbol{\mu}$ of molecule (1). The symmetry of the crystal thus gives rises to 8 possible dipole moment changes, $\Delta\boldsymbol{\mu}_i$ ($\pm\Delta\mu_a$, $\pm\Delta\mu_b$, $\pm\Delta\mu_c$). To each possible DBT insertion site we can thus associate one of these 8 $\Delta\boldsymbol{\mu}_i$ vectors. Note, however, that these 8 vectors all have equal magnitudes of $|\Delta\boldsymbol{\mu}|$. Upon application of an external electric field $\boldsymbol{E}$ with components (E_a, E_b, E_c), we obtain 8 possible linear Stark effects with the shifts: $h\Delta\nu = -(\pm\Delta\mu_a E_a \pm \Delta\mu_b E_b \pm \Delta\mu_c E_c)$, i.e., 8 sub-populations of molecules with different Stark shifts. In the special case of a field situated in one of the planes, e.g. (*a, b*), $E_c = 0$ and we find only four sub-populations, $h\Delta\nu = -(\pm\Delta\mu_a E_a \pm \Delta\mu_b E_b)$. Similarly, for a field oriented along one of the crystal axes, e.g. the *a*-axis, we find only two sub-populations with shifts $h\Delta\nu = \mp\Delta\mu_a E_a$. The cases of two and four distinct sub-populations are observed experimentally (see Figure 4). Finally, we note that, according to calculations, $\Delta\mu$ can have a significant component along the *c* axis, but the effective electric field component E_c should be negligible in our experiment. A small angle between the crystal and the chip surface (1–5°), or a small displacement of the molecule with respect to the electrode plane, can account for the deviations in the order of 50–100 MHz/kVcm^{-1}. Because of the inhomogeneous broadening, these values are too small to be unambiguously determined experimentally.

4. Conclusions

We presented a new host-guest system for single-molecule fluorescence spectroscopy based on DBT in 2,3-dibromonaphthalene (DBN). The system is the first successful demonstration of a strategy to use an asymmetric and polar host matrix to induce large static dipole moments in otherwise centrosymmetric guest molecules. This strategy leads to a large linear Stark effect in the order of 1.5 GHz/kVcm^{-1} for DBT in DBN. DBT molecules in the system behave remarkably well – they all respond similarly to the applied electric field, showing at the same time excellent spectral stability and narrow single-molecule resonances of about 40 MHz width. Our results were further complemented by quantum chemistry calculations, which indicated host-induced symmetry breaking in DBT molecules. By considering the symmetry of the host crystal, we have explained why embedding of DBT in DBN crystal, while exhibiting a single spectroscopic site, can lead to up to 8 different Stark coefficients in an applied electric field with arbitrary orientation. This system is an excellent candidate for single-molecule spectroscopy of DBT – an increasingly popular single-photon emitter. In addition, the large and homogeneous linear Stark response of the probe could be used for sensing local electric fields and for a precise tuning of the single-molecule emission wavelength over a large spectral range.

Acknowledgements

This work was partially supported by the National Science Centre, Poland, grant no. 2015/17/B/ST2/01744. The authors acknowledge financial support from NWO (The Netherlands Organization for Scientific Research) and its physics branch, the former FOM (Foundation for Fundamental Research on Matter), and the EraNET Cofund Initiative QuantERA under the European Union's Horizon 2020 Research and Innovation Programme (grant agreement no. 731473).

Conflict of Interest

The authors declare no conflict of interest.

Keywords: single-molecule spectroscopy · linear Stark effect · induced dipole moment · insertion sites · density functional calculations

[1] B. Lounis, W. E. Moerner, *Nature* **2000**, *407*, 491–493.
[2] Y. L. A. Rezus, S. G. Walt, R. Lettow, A. Renn, G. Zumofen, S. Götzinger, V. Sandoghdar, *Phys. Rev. Lett.* **2012**, *108*, 093601.

[3] G. Wrigge, I. Gerhardt, J. Hwang, G. Zumofen, V. Sandoghdar, *Nat. Phys.* **2008**, *4*, 60–66.
[4] C. Hettich, C. Schmitt, J. Zitzmann, S. Kühn, I. Gerhardt, V. Sandoghdar, *Science* **2002**, *298*, 385–389.
[5] T. Basché, W. E. Moerner, M. Orrit, U. P. Wild, Eds., *Single Molecule Optical Detection, Imaging and Spectroscopy*, VCH, Weinheim, **1997**.
[6] W. E. Moerner, M. Orrit, *Science* **1999**, *283*, 1670–1676.
[7] Y. Tian, P. Navarro, M. Orrit, *Phys. Rev. Lett.* **2014**, *113*, 135505.
[8] U. P. Wild, F. Güttler, M. Pirotta, A. Renn, *Chem. Phys. Lett.* **1992**, *193*, 451–455.
[9] M. Orrit, J. Bernard, A. Zumbusch, R. I. Personov, *Chem. Phys. Lett.* **1992**, *196*, 595–600.
[10] C. Brunel, P. Tamarat, B. Lounis, J. C. Woehl, M. Orrit, *J. Phys. Chem. A* **1999**, *103*, 2429–2434.
[11] F. Kulzer, R. Matzke, C. Bräuchle, T. Basché, *J. Phys. Chem. A* **1999**, *103*, 2408–2411.
[12] P. Bordat, M. Orrit, R. Brown, A. Würger, *Chem. Phys.* **2000**, *258*, 63–72.
[13] T. Y. Latychevskaia, A. Renn, U. P. Wild, *Chem. Phys.* **2002**, *282*, 109–119.
[14] M. Bauer, L. Kador, *J. Lumin.* **2002**, *98*, 75–79.
[15] M. Bauer, L. Kador, *J. Phys. Chem. B* **2003**, *107*, 14301–14305.
[16] P. Bordat, R. Brown, *Chem. Phys. Lett.* **2000**, *331*, 439–445.
[17] T. Plakhotnik, *ChemPhysChem* **2006**, *7*, 1699–1704.
[18] T. Plakhotnik, *J. Lumin.* **2007**, *127*, 235–238.
[19] S. Faez, S. J. van der Molen, M. Orrit, *Phys. Rev. B* **2014**, *90*, 205405.
[20] A. A. L. Nicolet, C. Hofmann, M. A. Kol'chenko, B. Kozankiewicz, M. Orrit, *ChemPhysChem* **2007**, *8*, 1215–1220.
[21] P. Türschmann, N. Rotenberg, J. Renger, I. Harder, O. Lohse, T. Utikal, S. Götzinger, V. Sandoghdar, *Nano Lett.* **2017**, *17*, 4941–4945.
[22] P. Lombardi, A. P. Ovvyan, S. Pazzagli, G. Mazzamuto, G. Kewes, O. Neitzke, N. Gruhler, O. Benson, W. H. P. Pernice, F. S. Cataliotti, C. Toninelli, *ACS Photonics* **2017**, *5*, 126–132
[23] D. Wang, H. Kelkar, D. Martin-Cano, T. Utikal, S. Götzinger, V. Sandoghdar, *Phys. Rev. X* **2017**, *7*, 021014.
[24] S. Pazzagli, P. Lombardi, D. Martella, M. Colautti, B. Tiribilli, F. S. Cataliotti, C. Toninelli, *ACS Nano* **2018**, *12*, 4295–4303.
[25] C. Kurtsiefer, S. Mayer, P. Zarda, H. Weinfurter, *Phys. Rev. Lett.* **2000**, *85*, 290–293.
[26] X. Ding, Y. He, Z.-C. Duan, N. Gregersen, M.-C. Chen, S. Unsleber, S. Maier, C. Schneider, M. Kamp, S. Höfling, *Phys. Rev. Lett.* **2016**, *116*, 020401.
[27] I. Aharonovich, D. Englund, M. Toth, *Nat. Photonics* **2016**, *10*, 631–641.
[28] A. A. L. Nicolet, P. Bordat, C. Hofmann, M. A. Kol'chenko, B. Kozankiewicz, R. Brown, M. Orrit, *ChemPhysChem* **2007**, *8*, 1929–1936.
[29] S. Faez, N. R. Verhart, M. Markoulides, F. Buda, A. Gourdon, M. Orrit, *Faraday Discuss.* **2015**, *184*, 251–262.
[30] Y. Tian, P. Navarro, B. Kozankiewicz, M. Orrit, *ChemPhysChem* **2012**, *13*, 3510–3515.
[31] M. Białkowska, W. Chaladaj, A. Makarewicz, B. Kozankiewicz, *Acta Phys. Pol. A* **2015**, *128*, RK.3.1.
[32] M. Białkowska, W. Chaładaj, I. Deperasińska, A. Drzewiecka-Antonik, A. E. Koziol, A. Makarewicz, B. Kozankiewicz, *RSC Adv.* **2017**, *7*, 2780–2788.
[33] Gaussian 09, Revision B.01, M. J. Frisch, G. W. Trucks, H. B. Schlegel, G. E. Scuseria, M. A. Robb, J. R. Cheeseman, G. Scalmani, V. Barone, B. Mennucci, G. A. Petersson, H. Nakatsuji, M. Caricato, X. Li, H. P.Hratchian, A. F. Izmaylov„ J. Bloino, G. Zheng, J. L. Sonnenberg, M. Hada, M. Ehara, K. Toyota, R. Fukuda, J. Hasegawa, M. Ishida, T. Nakajima, Y. Honda, O. Kitao, H. Nakai, T. Vreven, Jr. J. A. Montgomery, J. E. Peralta, F. Ogliaro, M. Bearpark, J. J. Heyd, E. Brothers, K. N. Kudin, V. N. Staroverov, T. Keith, R. Kobayashi, J. Normand, K. Raghavachari, A. Rendell, J. C. Burant, S. S. Iyengar, J. Tomasi, M. Cossi, N. Rega, J. M. Millam, M. Klene, J. E. Knox, J. B. Cross, V. Bakken, C. Adamo, J. Jaramillo, R. Gomperts, R. E. Stratmann, O. Yazyev, A. J. Austin, R. Cammi, C. Pomelli, J. W. Ochterski, R. L. Martin, K. Morokuma, V. G. Zakrzewski, G. A. Voth, P. Salvador, J. J. Dannenberg, S. Dapprich, A. D. Daniels, O. Farkas, J. B. Foresman, J. V. Ortiz, J. Cioslowski, D. J. Fox, *Gaussian Inc., Wallingford CT*, 2010
[34] I. Deperasińska, B. Kozankiewicz, *Chem. Phys. Lett.* **2017**, *684*, 208–211.
[35] C. R. Groom, I. J. Bruno, M. P. Lightfoot, S. C. Ward, *Acta Crystallogr. Sect. B Struct. Sci. Cryst. Eng. Mater.* **2016**, *72*, 171–179.
[36] P. Türschmann, N. Rotenberg, J. Renger, I. Harder, O. Lohse, T. Utikal, S. Götzinger, V. Sandoghdar, ArXiv:1702.05923v1 *Cond-Mat Physics* **2017**.
[37] I. Deperasińska, E. Karpiuk, M. Banasiewicz, B. Kozankiewicz, *Chem. Phys. Lett.* **2010**, *492*, 93–97.

Manuscript received: October 9, 2018
Revised manuscript received: November 7, 2018
Version of record online: November 28, 2018